

Journal of Biomedical Optics

SPIEDigitalLibrary.org/jbo

Ultrathin single-channel fiberscopes for biomedical imaging

Angelique Kano
Andrew R. Rouse
Arthur F. Gmitro



SPIE

Ultrathin single-channel fiberscopes for biomedical imaging

Angelique Kano, Andrew R. Rouse, and Arthur F. Gmitro

University of Arizona, College of Optical Sciences and Department of Medical Imaging, Tucson, Arizona

Abstract. Ultrathin flexible fiberscopes typically have separate illumination and imaging channels and are available in diameters ranging from 0.5 to 2.5 mm. Diameters can potentially be reduced by combining the illumination and imaging paths into a single fiberoptic channel. Single-channel fiberscopes must incorporate a system to minimize Fresnel reflections from air–glass interfaces within the common illumination and detection path. The Fresnel reflection at the proximal surface of the fiber bundle is particularly problematic. This paper describes and compares methods to reduce the background signal from the proximal surface of the fiber bundle. Three techniques are evaluated: (1) antireflective (AR)-coating the proximal face of the fiber, (2) incorporating crossed polarizers into the light path, and (3) a novel technique called numerical aperture sharing, whereby a portion of the image numerical aperture is devoted to illumination and a portion to detection. © 2013 Society of Photo-Optical Instrumentation Engineers (SPIE) [DOI: 10.1117/1.JBO.18.1.016013]

Keywords: endoscopy; fiber bundle; catheter; background; Fresnel; fiberscope; numerical aperture; polarization; antireflective coating.

Paper 12515 received Aug. 13, 2012; revised manuscript received Dec. 3, 2012; accepted for publication Dec. 10, 2012; published online Jan. 18, 2013.

1 Introduction

Clinical endoscopes are used to visualize tissues located inside the body. To accomplish this, an endoscope must deliver light to the tissue and collect the diffusely reflected light. A typical endoscope has an imaging channel, one or more illumination channels, an instrument channel, and an air/water delivery channel.¹

The illumination channels typically consist of optical fibers or fiber bundles coupled to a bright external white-light source. Image contrast is based on variations in the strength and spectral content of reflected (or backscattered) light. Color is an important visual cue for diagnosis because pathology often has modified biochemistry resulting in alterations to molecular distributions and associated tissue optical properties.

Modern flexible endoscopes are of two types: videoscopes and fiberscopes. In a videoscope, a lens collects the diffusely reflected light from the tissue and focuses it onto a video detector located within the tip of the videoscope. Videoscopes produce high-quality images, but are relatively large owing to the size of the detector. Endoscopes with diameters smaller than 2.5 mm are typically fiberscopes. Fiberscopes use a bundle of optical fibers to relay an image from the distal to the proximal end of the catheter. Often, a graded-index (GRIN) lens at the distal end of the fiberscope is used to image the tissue surface onto the input face of the fiber bundle. On the proximal end, the fiber face is imaged onto a camera or viewed through an ocular by the user.

Fiberscopes can be very small and flexible. However, the number of resolvable picture elements in a fiberscope image is limited by the number of fibers in the bundle and, therefore, there is a trade-off between the diameter of the scope and the number of picture elements in the image. Fiber bundles used in modern fiberscopes are at or near the theoretical limit on

the packing density of individual fibers.^{2–4} Thus, ultrathin fiberscopes with diameters of 0.5 mm are limited to only a few thousand picture elements. For example, one of the smallest commercially available fiberscopes is the 0.5-mm-diameter Olympus AF-5, which has only 4000 picture elements.⁵

One way to increase the resolution and/or space-bandwidth product (number of image pixels) of a fiberscope, without impacting its overall size, is to use the fiber bundle for both the illumination path and the detection path. In such a single-channel fiberscope, unwanted Fresnel reflections from air–glass interfaces within the optical system become problematic. To achieve high image quality, the worst of these offenders, the Fresnel reflection at the proximal surface of the fiber, must be reduced. In this paper, we describe and evaluate three techniques to reduce this background in ultrathin single-channel fiberscopes.

2 Basic Single-Channel Fiberscope

Figure 1 shows a single-channel fiberscope where a beamsplitter has been inserted to couple illumination into the fiberoptic imaging bundle. An objective focuses the illumination onto the input face of the fiber bundle, which relays the illumination light to the distal end of the catheter. A GRIN lens distributes the illumination light over the object. The diffusely reflected light from the object is collected by the GRIN lens and relayed back to the optical system by the fiber bundle. The light passes through the objective and beamsplitter and is focused onto a detector by a camera lens.

To characterize this single-channel fiberscope, one must properly describe the measured signal. The signal out of the detector can be separated into object (S_{object}) and background (S_{back}) components. The background signal may be further divided into (1) the dark-charge noise level of the camera, (2) stray light and ghost reflections in the illumination path, and (3) backscattered light and Fresnel reflections from the

Address all correspondence to: Andrew R. Rouse, University of Arizona, College of Optical Sciences and Department of Medical Imaging, Tucson, Arizona. Tel: +520 626 4720; E-mail: gmitro@radiology.arizona.edu

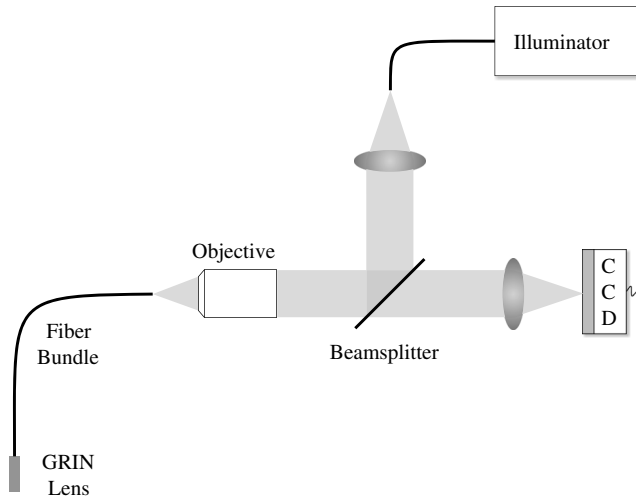


Fig. 1 Basic single-channel fiberscope.

fiber bundle/GRIN lens combination (catheter background). The first two background signals are typically low compared to the catheter background. As such, these signals are not included in this analysis, which considers only background arising from the catheter (fiber/GRIN lens combination). For a more detailed discussion of dark charge, stray light, and ghost reflections, see Ref. 6.

The model of the single-channel fiberscope breaks the optical layout into three compartments: the catheter, the coupling optics, and the detector (Fig. 2). The object signal and catheter background signal for the basic single-channel fiberscope are

$$S_{\text{object}} = M_{\text{object}} T_{\text{cpl}} D \quad (1)$$

and

$$S_{\text{back}} = M_{\text{back}} T_{\text{cpl}} D, \quad (2)$$

where M_{object} and M_{back} are the radiant exitances from the proximal fiber bundle surface for the object and background, respectively. The variable T_{cpl} is an energy transfer term encompassing the transmission and magnification of the imaging system between the fiber bundle and the detector. The factor D describes the mapping of the irradiance on the charge coupled device (CCD) to a digital output value.

Light associated with both the object and catheter background can be expressed as a function of E_{prox} , the irradiance of the illumination light incident at the proximal surface of the fiber bundle over the collection angles of the fiber bundle. For this paper, it will be assumed that the illumination is uniformly distributed over the proximal fiber face. At each interface throughout the catheter, some portion of this light will be reflected and the rest transmitted (surface absorption is neglected). Reflected or backscattered light from the catheter will contribute to the background signal.

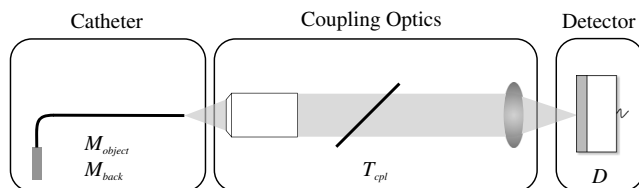


Fig. 2 Compartmentalized model of the optical components in the single-channel fiberscope.

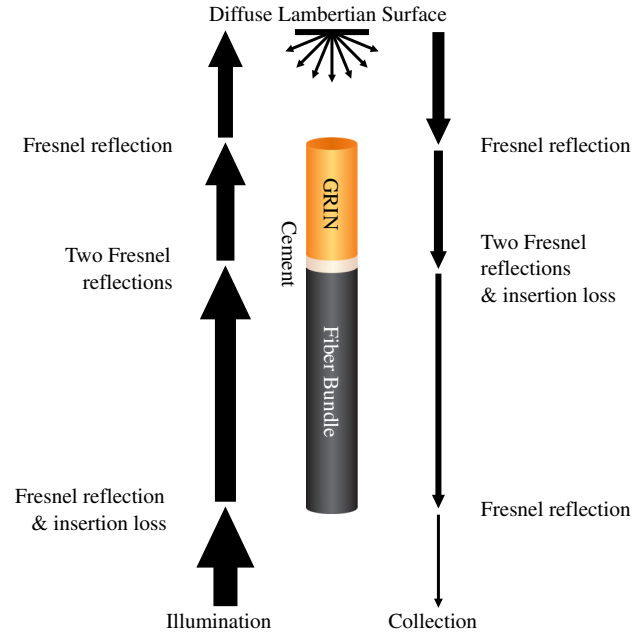


Fig. 3 Losses in the expected object signal of a fiberscope. Linewidth of arrows indicates the transmission values across each interface as well as transmission efficiencies through materials.

2.1 Object Signal

As shown in Fig. 3, illumination light incident on the proximal face of the fiber bundle passes through an air–fiber interface where a portion of the light is reflected. Of the light transmitted through the air–fiber interface, only a fraction is coupled into the fiber and transmitted to the distal end. The fiber couples the light with an efficiency $\tau_{\text{fb-illum}}$, which is associated with the fiber packing fraction as well as the numerical aperture (NA) of the fiber bundle.^{6,7} Some of the light will be absorbed (or attenuated) in the fiber, and a small fraction is backscattered as light propagates through the fiber bundle. At the distal end of the fiber bundle, the illumination light reaches the fiber/cement/GRIN lens junction, where the light will encounter losses from Fresnel reflections and material absorptions. The distal surface of the GRIN lens is often antireflective (AR)-coated to minimize back reflections at the GRIN–air interface.

The illumination light exiting the lens will be distributed over an object area determined by the magnification of the GRIN lens. We model the object as a Lambertian reflector. Thus light incident at the object surface will be diffusely reflected into a solid angle of 2π steradians. Reflected light collected by the GRIN lens will experience loss as it once again passes through each interface in the catheter. The light reenters the fiber bundle with collection-coupling efficiency $\tau_{\text{fb-coll}}$. The radiant exitance from the object at the proximal fiber surface is

$$M_{\text{object}} = \tau_{\text{fb-illum}} \tau_{\text{fb-col}} T_{\text{catheter}} \frac{R_{\text{object}} NA_{\text{fb}}}{m^2} E_{\text{prox}}, \quad (3)$$

where T_{catheter} is a transmission term that incorporates the losses due to the four Fresnel reflections (two on either end of the fiber and GRIN lens) and three material absorptions (fiber, cement, and GRIN lens) within the catheter. M_{object} is directly proportional to the illumination incident on the proximal face of the fiber bundle E_{prox} , the reflectivity of the object R_{object} , and the square of the NA of the fiber bundle NA_{fb} . M_{object} is

inversely proportional to the square of the magnification of the GRIN lens m , from fiber bundle to object space.

The radiant exitance, M_{object} , will be a small fraction of the incident irradiance E_{prox} , due to low tissue reflectivity, low collection NA, and high magnification in endoscopic imaging systems. This highlights the need to minimize background reflections that are significant relative to the object signal.

2.2 Background Signal

Each interface in the catheter will generate a Fresnel reflection leading to unwanted background light. The three primary sources of reflections are (1) the proximal air–fiber interface, (2) the distal fiber–GRIN interface, and (3) the distal GRIN–air interface. The latter two reflections can be minimized by using index-matching optical cement and an appropriate AR coating on the GRIN lens, respectively. The most critical source of background signal for a single-channel fiberscope is the Fresnel reflection at the proximal air–fiber interface.

The radiant exitance at the proximal surface of the fiber due to the background can be expressed as

$$M_{\text{back}} = M_{\text{prox-refl}} + M_{\text{dist-cath}}, \quad (4)$$

where $M_{\text{prox-refl}}$ represents the problematic proximal reflection and $M_{\text{dist-cath}}$ represents all the other sources of background signal in the catheter. $M_{\text{prox-refl}}$ can further be expressed as

$$M_{\text{prox-refl}} = R_{\text{air-fb}} E_{\text{prox}}, \quad (5)$$

where $R_{\text{air-fb}}$ is the reflection coefficient associated with the air–fiber-bundle interface.

2.3 Image Contrast

The main challenge in fabricating a single-channel fiberscope for conventional reflectance white-light imaging lies in reducing the high background-signal levels relative to the typically low object-signal levels. Fresnel reflections from the fiber bundle lower image contrast to a level that is typically unacceptable for practical use. The signal-to-background ratio (SBR), defined as the ratio of the object signal (S_{object}) to the background signal (S_{back}), is a measure that can be used to quantify this problem.

In principle, the background signal can be subtracted from the image. However, the unwanted signal uses up valuable dynamic range and contributes noise to the resulting background-subtracted image. In the case where the detector output is limited by photon noise, the noise standard deviation varies as the square root of the number of incident photons, N (Ref. 8), which includes contributions from the object signal and the background. The signal-to-noise ratio (SNR) as a function of SBR is

$$\text{SNR} = \sqrt{N} \frac{\text{SBR}}{1 + \text{SBR}}. \quad (6)$$

In the case of very low, almost negligible, background the $\text{SBR} > 1$ and the SNR approaches \sqrt{N} . When $\text{SBR} \ll 1$, the factor $\frac{\text{SBR}}{1 + \text{SBR}} \approx \text{SBR}$ and the $\text{SNR} \approx \sqrt{N}\text{SBR}$. Typically an imaging system requires an SBR of at least 1 to produce acceptable images ($\text{SNR} = 0.5\sqrt{N}$). Unfortunately, the low object-signal collection efficiency and high background of the basic single-channel fiberscope (Fig. 1) results in images that typically have an $\text{SBR} \ll 1$. Therefore this system does not perform

well without significantly reducing the background signal originating from the Fresnel reflection at the proximal fiber surface.

3 Reducing Background from Proximal Fiber Face

Three techniques were investigated to reduce the background arising at the proximal face of the fiber bundle: (1) AR coating, (2) crossed polarizers, and (3) a technique called NA-sharing whereby a portion of the numerical aperture is devoted to illumination and a portion to signal detection. The following subsections describe the modifications that must be made to the system introduced in Sec. 2 to properly model these three techniques.

3.1 Antireflection Coating

An AR coating on the proximal fiber surface is one method to reduce the catheter background signal. A perfect AR coating would result in the least amount of loss to both the incident illumination and the detected image signal. Unfortunately, AR coatings are not perfect and there will always be some amount of residual reflection at the coated surface. To model this situation, the transmission coefficient, T_{catheter} , in Eq. (3) and the reflection coefficient, $R_{\text{air-fb}}$, in Eq. (5) are altered due to the AR coating. This yields an increased transmission and a decreased reflection of the beams entering and exiting the proximal face of the fiber bundle. The object and background signals for this situation become

$$S_{\text{object-AR}} = M_{\text{object-AR}} T_{\text{cpl}} D \quad (7)$$

and

$$S_{\text{back-AR}} = (M_{\text{prox-refl-AR}} + M_{\text{dist-cath-AR}}) * T_{\text{cpl}} D, \quad (8)$$

where the AR subscript denotes variables and coefficients that are specific to the AR-coated system.

3.2 Crossed Polarizers

Another way to reduce the background reflection from the proximal face of the fiber is by inserting crossed polarizers in the illumination/detection path. In general, polarization is maintained upon specular reflection from a surface. Thus crossed polarizers have a high extinction of the reflected signal from the input fiber face. Imaging fiber bundles do not maintain polarization on transmission, and thus the object signal and any background arising after the illumination enters the fiber bundle will be unpolarized. Crossed polarizers in the optical path therefore reduce the background signal from the proximal fiber surface relative to the other signal components.

Figure 4 shows the layout for a crossed-polarizer single-channel fiberscope. It is identical to the basic system except for the polarizing beamsplitter, which reflects s -polarized light and transmits p -polarized light. With the beamsplitter in place, the coupling optics in the detection path have a transmission $T_{\text{cpl-pol}}$ for the s -polarized proximal background reflection and a transmission $T_{\text{cpl-unpol}}$ for the unpolarized object signal and background components coming out of the catheter. The object and background signals for this situation are

$$S_{\text{object-pol}} = M_{\text{object}} T_{\text{cpl-unpol}} D \quad (9)$$

and

$$S_{\text{back-pol}} = M_{\text{prox-refl}} T_{\text{cpl-pol}} D + M_{\text{dist-cath}} T_{\text{cpl-unpol}} D, \quad (10)$$

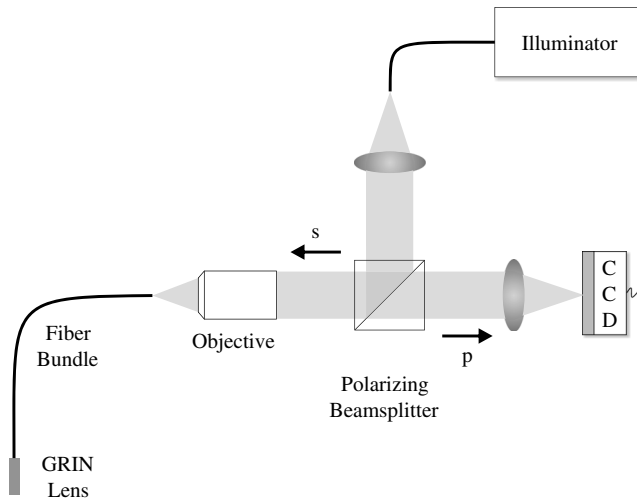


Fig. 4 A single-channel fiberscope with crossed polarizers.

where the pol subscript denotes variables and coefficients that are specific to the crossed-polarizer system.

In an ideal system, the proximal reflection would be completely rejected by the polarizing beamsplitter, which would eliminate the first term of Eq. (10). However, real polarizers always pass some small amount of the light they are designed to block. Therefore, to properly model the crossed-polarizer system one must characterize the s and p components of the light individually. Further description of this characterization is beyond the scope of this paper but a detailed analysis⁶ was used for all necessary calculations.

3.3 Numerical Aperture Sharing

Another way to reduce the amount of background signal collected from the proximal surface of the fiber bundle is called numerical aperture sharing. The idea is to dedicate a portion of the fiber bundle NA to illumination and a separate portion to signal collection. Figure 5 shows a conceptual layout for a single-channel fiberscope using the NA-sharing principle. A ring light source is baffled to pass only rays with angles that lie just inside the fiber bundle transmission cutoff angle. This hollow cone of rays reflects off a mirror with a central hole and converges onto the input face of the fiber. As depicted in

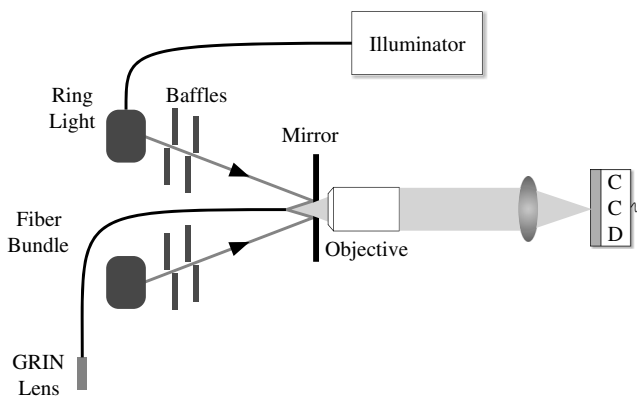


Fig. 5 A single-channel fiberscope using numerical aperture (NA)-sharing.

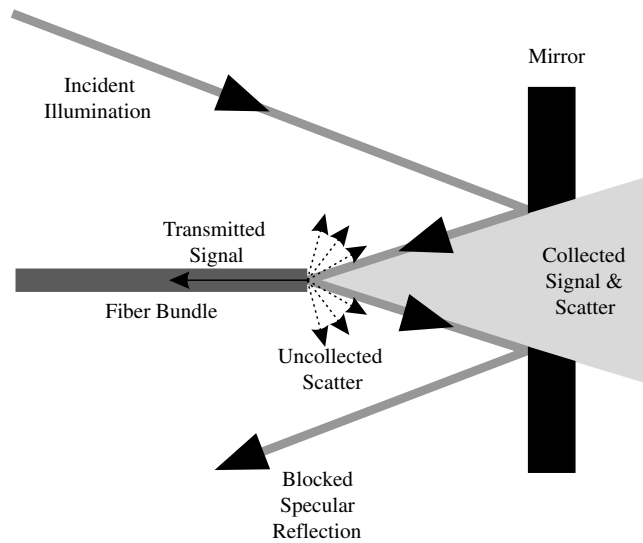


Fig. 6 Components of background signal at proximal fiber face for the NA-sharing system.

Fig. 6, the benefit of this method is that the proximal Fresnel reflection is blocked by the mirror and does not reach the CCD. The majority of the light returning back through the fiber passes through the central hole in the mirror and is imaged onto the detector. With proper alignment, the background from the proximal fiber face will be limited to surface scatter (i.e., no specularly reflected component). To model the NA-sharing scenario, the illumination coupling efficiency into the fiber bundle as well as the effect of the mirror on the collected signal must be incorporated.

The NA-sharing system illuminates the fiber at angles just inside the geometrical NA of the fiber bundle. High-resolution imaging fiber bundles propagate only a few modes, and the coupling efficiency decreases with increasing illumination angle.^{7,9} As a result, the coupling efficiency in the illumination path of the NA-sharing system is significantly lower than the coupling efficiency in the case where the NA of the fiber bundle is filled by the incoming illumination. In addition, the collection efficiency of the NA-sharing system is decreased because some portion of the light exiting the proximal surface of the fiber bundle will be blocked by the mirror. The fraction of light that is transmitted by the mirror/objective sub-assembly is represented by the transmission term, T_{mirror} .

Whereas the light entering the fiber in the NA-sharing system is limited to a narrow range of angles, the fibers within the bundle do not maintain those angles as light propagates within the fiber. Therefore, at the distal tip of the catheter the fiber bundle's NA is filled and the object is fully illuminated.

With the changes in coupling efficiency and mirror transmission, the object and background signals become

$$S_{\text{object-NA}} = M_{\text{object-NA}} T_{\text{mirror}} T_{\text{cpl}} D \quad (11)$$

and

$$S_{\text{back-NA}} = (M_{\text{prox-refl-NA}} + M_{\text{dist-cath-NA}} T_{\text{mirror}}) * T_{\text{cpl}} D, \quad (12)$$

where the NA subscript denotes variables and coefficients that are specific to the NA-sharing system. $M_{\text{prox-refl-NA}}$ is the radiant exitance associated with light scattered or reflected at the

proximal fiber surface that passes through the mirror to the CCD. A more detailed representation of this model can be found in Ref. 6.

4 Expected Performance of the Constructed Systems

We constructed three single-channel fiberscopes based on the methods presented in the previous section. Each system used a similar optical path with the addition and/or removal of a few optical elements.

This section describes the improvement in SBR expected with the three constructed systems over a basic system with an uncoated fiber bundle. For the case when nothing is done to reduce the reflection from the proximal surface of the fiber bundle, the modeled SBR is only 0.029, whereas under the ideal condition of zero background signal from the proximal fiber surface, the SBR is 1.09 in each system. The ideal no-background SBR is the same for all three systems because both the object and remaining background signals pass through the same optics including the catheter. These worst-case and best-case SBRs were obtained by using the detailed model developed to characterize our specific systems. The values are sensitive to various system parameters, most notably the working distance of the catheter and the reflectivity of the object. As such, the absolute numbers are unlikely to be relevant in a general sense. However, the values still allow us to compare the relative performance of the three systems, and this comparison will be applicable to other setups and applications.

4.1 AR-Coated Fiberscope

To test the concept of an AR-coated fiberscope, we built a system based on the basic single-channel fiberscope shown in Fig. 1. We used a 10% reflective (90% transmissive) beam-splitter in this system and applied an AR coating to the proximal surface of the fiber bundle catheter. The measured reflectance from the proximal surface of this catheter was 0.82%, which yields an expected SBR of 0.20. This is an improvement over the SBR of 0.029 obtained with an uncoated 3.9% proximal reflection. Nevertheless, the proximal reflection is still the dominant source of background.

4.2 Crossed-Polarizer Fiberscope

To investigate the use of crossed polarizers as a means to reduce the proximal reflection, we constructed a system based on the sketch shown in Fig. 4. Two additional elements (linear polarizers) were inserted into the beam path: a generator in the illumination path and an analyzer in the detection path. The polarizing beamsplitter¹⁰ reflects 99.5% of the *s*-polarized light and 1.8% of *p*-polarized light in the illumination beam. To improve the degree of illumination polarization, a generator¹¹ rotated to pass *s*-polarization was placed before the beamsplitter. In the detection path, the beamsplitter passes most of the *p* state along with a small amount of the unwanted *s* state. An analyzer was inserted before the camera lens to further reduce this unwanted *s*-polarized light. The analyzer also removes *s*-polarized internal reflections off the AR-coated surface of the beamsplitter cube.

In this configuration, the illumination degree of polarization (DOP) was 0.997 at the fiber plane, and the proximal background decreased to 0.01% of E_{prox} . This improvement in proximal background rejection increases the expected SBR to 0.81.

4.3 NA-Sharing Fiberscope

The system constructed to demonstrate the NA-sharing concept is shown in Fig. 5. It includes a ring light source with a 0.5 NA. The baffles consist of two sets of ring apertures that pass rays with angles ranging from 16.9 to 20.5 deg (NA range 0.29 to 0.35). As previously discussed, light incident on the fiber bundle in this high-NA range is coupled with substantially lower efficiency than would be expected under normal full-NA illumination. In our case, the transmission factor is 12% compared to 49% for a fully filled NA. On the detection side, the NA passed by the mirror is 0.28. Based on measurements, the mirror will pass 73% of the light coming out of the fiber bundle.

The NA-sharing system rejects the Fresnel reflection from the proximal surface of the fiber bundle to the extent that surface scatter becomes important to quantify. Some portion of this scattered light will make it through the central hole in the mirror and onto the detector. Based on scattering data for clean polished glass,⁶ one can estimate a residual background contribution from the proximal fiber surface of 0.006% of E_{prox} . In this case, the expected SBR is 0.85.

5 Measured Performance

There are a number of ways to evaluate and compare the performance of single-channel fiberscopes. The proximal reflections of the crossed-polarizer and NA-sharing techniques are approximately an order of magnitude lower than the proximal reflection of the AR-coated system. However, to do a true comparison between the three systems, one must use a metric, such as SBR, that is normalized to object signal. In addition to SBR, the illumination and detection throughput of the three systems may be important in some situations. Finally, the three techniques can be compared in terms of overall cost and ease of implementation.

5.1 Signal-to-Background Comparison

For each of the systems, the SBR can be calculated by collecting three different images. I_a is a raw image taken with the object at a prescribed working distance. I_b is a raw background image taken with the object removed. I_c is a stray light image taken with the source turned on but with the fiber bundle catheter removed. These three images are related mathematically to the true signal (S_{object}), the catheter background signal (S_{back}), and the background signal due to stray light and dark current ($S_{\text{detector-back}}$) as

$$\begin{aligned} I_a &= S_{\text{object}} + S_{\text{back}} + S_{\text{detector-back}}, & I_b &= S_{\text{back}} + S_{\text{detector-back}}, \\ I_c &= S_{\text{detector-back}}. \end{aligned} \quad (13)$$

The SBR is related to these three images by

$$\text{SBR} = \frac{S_{\text{object}}}{S_{\text{back}}} = \frac{I_a - I_b}{I_b - I_c}. \quad (14)$$

Images of text (the letter O) acquired with the three systems are shown in Fig. 7. The top row in Fig. 7 shows the raw image data (I_a) and the bottom row shows the background-subtracted images ($S_{\text{object}} = I_a - I_b$). A region of interest inside the letter O was used to measure the SBR of each of the three single-channel fiberscopes. In the case of the AR-coated system, a region of interest was selected that avoided the two parallel scratches running through the center of the images.

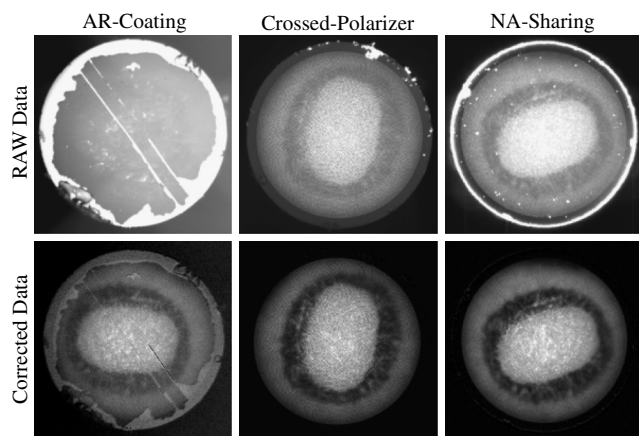


Fig. 7 Raw (top row) and background-subtracted (bottom row) images of the letter O on white printer paper taken by the antireflective-coated, crossed-polarizer, and NA-sharing fiberscopes.

Table 1 shows a comparison of the SBR for the three techniques. The first row gives the SBR for the three systems under the ideal condition of zero background signal from the proximal fiber surface. As mentioned previously, this ideal (no proximal background) SBR is 1.09 for each system. The second row contains the expected SBR based on the specifications for the optical components and values discussed in Sec. 4. The third row contains the SBR measured using the calculation methods described above.

We expected the measured SBRs in Table 1 to be slightly higher than the predicted values because the real object (paper) had a specular component with a slightly higher reflectivity than the Lambertian object in the model. This was observed for the crossed-polarizer and NA-sharing systems. However, for the AR-coated fiberscope, we measured an SBR that was significantly lower than the expected value. We attribute this discrepancy to the damaged AR coating on the fiber bundle (some damage is evident in the AR-coated results shown in Fig. 7).

All of the single-channel fiberscopes reduced the background signal caused by the proximal fiber surface. For the crossed-polarizer and NA-sharing fiberscopes, this reduction was quite significant. In fact, the proximal reflection is no longer the dominant contributor to the overall background signal for these two systems. To determine the most significant contributor to the remaining background signal, we calculated the relative contribution for each background component normalized to the object signal, i.e., $\frac{S_{\text{prox-refl}}}{S_{\text{object}}}$. Table 2 shows the resulting values for each of the fiberscopes. Normalizing by the object signal removes the dependence on the incident power, allowing for a direct

Table 1 Signal-to-background ratio (SBR) comparison for the three methods.

	Antireflective (AR) coating	Crossed polarizers	Numerical aperture (NA) sharing
No proximal reflection	1.09	1.09	1.09
Expected	0.20	0.81	0.85
Measured	0.13	0.92	1.03

Table 2 Background signal components normalized to the object signal.

	Uncoated	AR coating	Crossed polarizers	NA-sharing
Proximal air-fiber reflection	34.2	7.18	0.35	0.24
Fiber internal backscatter	~0	~0	~0	~0
Distal fiber-cement reflection	0.003	0.003	0.003	0.003
Distal cement-GRIN reflection	0.19	0.19	0.19	0.19
Distal GRIN-AR coating reflection	0.54	0.54	0.54	0.54
Resulting SBR	0.03	0.13	0.92	1.03

comparison between the three systems. It also removes losses that occur in both the image and background component signals, e.g., transmission of the beamsplitter, transmission of the GRIN lens and cement, and coupling efficiency into the fiber bundle. In the better-performing crossed-polarizer and NA-sharing fiberscopes, the largest source of background is the reflection off the AR-coated surface of the GRIN lens.

5.2 Throughput Comparison

Each of the three techniques presented in this paper can reduce the amount of background signal from the proximal surface. In the case of the crossed-polarizer and NA-sharing systems, the residual surface contribution is similar. To investigate whether there is an inherent advantage to using one technique over the other, we should also investigate the light efficiency of the three systems.

Table 3 shows the efficiency of the crossed-polarizer and NA-sharing systems relative to the AR-coated system. By normalizing the better-performing crossed-polarizer and NA-sharing systems to the AR-coated system, one can easily see the relative performance of the three techniques. The first row in Table 3 covers the illumination path beginning at the input of the source light guide (same source for all three systems) and ending just outside the proximal surface of the fiber bundle. Therefore, these numbers describe how efficient the three systems are at delivering light to the proximal face of the fiber bundle. The crossed-polarizer fiberscope is the most efficient at 3.1

Table 3 Throughput comparison of the three methods. The efficiencies for the crossed-polarizer and NA-sharing systems are normalized to the AR-coated system values.

	Crossed polarizers	NA-sharing
Illumination efficiency	3.10	0.42
Coupling efficiency	0.97	0.24
Imaging efficiency	0.29	0.66
Total efficiency	0.87	0.07

times that of the AR-coated system. The NA-sharing system is the least efficient at only 0.42 times that of the AR-coated system. It is important to point out that these numbers are highly dependent on certain system components. For example, our AR-coated system had a relatively low illumination efficiency because it employed a 10% reflective beamsplitter.

The second row in Table 3 covers the relative efficiencies of the three systems with respect to coupling the illumination into the fiber. These efficiencies are affected by the reflectivity of the proximal fiber face as well as the ability of the fiber to accept and transmit the NA profile of the illumination. The AR-coated and crossed-polarizer systems fill the NA of the fiber bundle and therefore have coupling efficiencies that differ only slightly due to the ARcoating. As previously described, the NA-sharing system illuminates the fiber in a narrow range of angles near the maximum acceptance angle of the fiber. As expected, the trade-off in this system is a fairly low coupling efficiency of roughly one quarter that of the other two systems.

Light then travels through the catheter, interacts with the object, is collected by the distal optics, and travels back through the catheter to the proximal surface of the fiber bundle. Each of these interactions is identical for the three techniques. The third row of Table 3 compares the ability of each system to transfer the collected light just inside the proximal face of the fiber bundle to the detector. Unfortunately, it is impossible to measure the amount of light inside the fiber, and any attempt to measure the light coming out of the proximal fiber face necessarily blocks the illumination. However, assuming identical catheters and objects between the three systems, the illumination emanating from the distal tip of the catheter is an excellent representation of the signal returning to the camera just before it escapes from the proximal tip of the fiber bundle. As shown in Table 3, the crossed-polarizer and NA-sharing systems have imaging efficiencies that are 0.29 and 0.66 times that of the AR-coated fiberscope, respectively.

The final row of Table 3 compares total efficiency, which is the product of the illumination, coupling, and imaging efficiencies of a particular system. This analysis shows that the AR-coated fiberscope is the most efficient system and that the NA-sharing system is the least efficient. However, even with their poorer throughput efficiencies, the SBR results indicate that the crossed-polarizer and NA-sharing systems are better at producing high-contrast images. Based on these results, the choice between imaging systems may depend on the specific application. The NA-sharing system will produce the best SBR and therefore the highest-contrast images. However, in light-starved applications, it may be better to take a minor hit in SBR in exchange for the significant increase in light efficiency provided by the crossed-polarizer system.

5.3 Practical Considerations

Another way of comparing the three systems is to review the practical aspects of constructing, aligning, and characterizing the systems. The crossed-polarizer system is constructed from standard optical components, whereas the AR-coated system requires a specially coated fiber bundle and the NA-sharing fiberscope uses custom machined baffles and a custom mirror. Cost-wise, the components for the crossed-polarizer system are more expensive but are likely to be more flexible to changes in the design. The AR-coated fiberscope is the easiest to align, whereas the alignment of the NA-sharing system is the most

challenging, as the entire principle is dependent on careful positioning of the fiber bundle with respect to the ring light source and mirror.

6 Discussion

An important factor that limits the SBR is the collection efficiency of light from the object. While tissue can have a specular component, it is essentially a Lambertian emitter.^{12,13} For the catheters built during this study, the collection efficiency from a Lambertian reflector at a working distance of 1.5 mm is only 2.2%. Obviously the collection efficiency worsens with increased working distance or lower reflectivity, both of which may be encountered when imaging some tissues. Unfortunately, this fact is largely unavoidable, and successful *in vivo* use of a single-channel fiberscope will likely require a further reduction in the background signal.

Even though the AR-coated fiberscope was the most light-efficient of the three systems, it achieved the lowest SBR improvement due to the residual reflectance from the proximal fiber surface. To increase the SBR of the AR-coated system to a level comparable with the other two techniques would require a proximal reflection < 0.07% (SBR = 0.85), which is unrealistic. Thus the next logical step is to further improve the performance of the NA-sharing and/or crossed-polarizer fiberscopes. This might be accomplished through the use of higher quality polarizers in the crossed-polarizer system or further improvements in the baffle and mirror assembly of the NA-sharing system. In addition, one might effectively combine two systems by using an AR-coated fiber in a crossed-polarizer or NA-sharing setup.

After the proximal surface reflection, the next largest source of background in the three systems is the distal AR-coated surface of the GRIN lens. Although a residual reflectance of 0.47% is low, an even better coating would improve the SBR ratio. However, the materials used to manufacture GRIN lenses limit the quality of the available AR coatings.¹⁴ A further reduction in this distal reflection may require replacing the GRIN lens with a different miniature optical component. It is important to note that this study was performed with the endoscope and object in an air space. When imaging in a liquid environment, the glass-air AR coating on the GRIN lens would be replaced with a glass-water AR coating. The resulting change in reflectivity of the distal GRIN interface will clearly lead to slightly different SBRs than those reported in this paper.

The model presented in this paper does not specifically account for losses in the optical system caused by bends in the flexible fiber bundle. Each of the three constructed systems included an approximately 90-deg bend in the catheter. This bend slightly increased the losses incurred by light traveling in both directions through the bundle. However, since the individual fibers in the bundle support only a few modes, one can assume that the light propagating down the length of the fiber bundle is identical in each of the three systems once normalized for differences in overall power. Therefore, any deleterious effects caused by the 90-deg bend were common to all three systems and the comparison presented in this paper is still valid. In addition, these losses are insignificant compared to the proximal fiber-air and distal GRIN-air reflections.

One additional method to reduce the proximal fiber-air background reflection is to polish a known angle into the proximal face of the fiber. Alignment of such a system would involve tilting the source and the detector to maintain focus throughout the

field, and one would expect some loss in coupling efficiency due to the oblique fiber face. How this tilted illumination approach compares to the three methods described in this paper is a topic for future study.

7 Conclusions

The fiberscopes presented in this paper represent an attempt to improve on ultrathin fiberscope technology by incorporating the illumination and imaging paths into a single fiber bundle channel. Simply combining the two light paths via a beamsplitter results in poor imaging performance due to a high background signal from the Fresnel reflection at the proximal surface of the fiber bundle. We identified and characterized three systems that reduce the proximal Fresnel reflection: (1) AR coating the proximal fiber face, (2) incorporating crossed polarizers into the light path, and (3) a novel technique called NA-sharing, whereby a portion of the image numerical aperture is devoted to illumination and a portion to detection.

The results show that an AR-coated single-channel fiberscope, while the most light efficient, is inferior in terms of SBR unless the residual reflectance from the proximal fiber surface is $<0.07\%$. Unfortunately, such a low residual reflectance from an AR-coated fiber bundle is unattainable using currently available technology. The crossed-polarizer system is the most light efficient, but the NA-sharing system is superior in terms of SBR because it virtually eliminates the proximal Fresnel reflection. The lower illumination efficiency of the NA-sharing system compared with the crossed-polarizer system may be a problem for light-starved applications.

Which technology to employ in a given system will depend on the system requirements and the application. It may be that a combination of an AR-coated fiber with either the crossed-polarizer or NA-sharing system will be the best solution.

Acknowledgments

This research was supported by NIH Grants CA113964 and CA115780.

References

1. M. V. Sivak, Jr., *Gastroenterologic Endoscopy*, vols. **1 and 2**, 2nd ed., W. B. Saunders, Philadelphia, PA (2000).
2. K. L. Reichenbach and C. Xu, "Numerical analysis of light propagation in image fibers or coherent fiber bundles," *Opt. Express* **15**(5), 2151–2165 (2007).
3. Fujikura America, Santa Clara, CA, "Fujikura image guide specifications," www.fai.fujikura.com/prod/imagefiber/p1_1.
4. Sumitomo Electric USA, Torrance, CA, "Coherent Fiber Bundle," part number: IGN-05/10, www.sumitomoelectricusa.com.
5. T. Hatori, Endoscope, U. S. Patent No. 4,805,596 (1989).
6. A. L. Kano, "Ultrathin single and multi-channel fiberscopes for biomedical imaging," Ph.D. Thesis, University of Arizona (August 2009).
7. J. A. Udovich et al., "Spectral background and transmission characteristics of fiber optic imaging bundles," *Appl. Phys.* **27**(25), 4560–4568 (2008).
8. W. L. Wolfe, *Introduction to Radiometry*, Vol. **TT29**, SPIE Press, Bellingham, WA (1998).
9. C. R. Pollock, *Fundamentals of Optoelectronics*, Richard D. Irwin, Chicago, IL (1995).
10. M. Griot, "Part no. PBSH-450-700-100," CVI Melles Griot., Albuquerque, NM, www.cvimellesgriot.com.
11. M. Griot, "Part no. 03 FPC 005," CVI Melles Griot., Albuquerque, NM, www.cvimellesgriot.com.
12. T. T. Goodell et al., "In vivo determination of optical properties of normal and tumor tissue with white light reflectance and an empirical light transport model during an endoscopy," *J. Biomed. Opt.* **10**(3), 034018 (2005).
13. E. J. Seibel, R. S. Johnston, and E. S. Barhoum, "Optical modeling of an ultrathin scanning fiber endoscope, a preliminary study of confocal versus non-confocal," *Opt. Express* **13**(19), 7548–7562 (2005).
14. GRINTECH GmbH., GRINTECH GmbH, Jena, Germany, Part number: GFRL-050-cust-C1," www.grintech.de, Gradient index lens.